

Title: Plant wax isotopes in Greenland lakes record widespread CH₄ uptake during Holocene warming

Authors: J.M. McFarlin^{1,2*}, Y. Axford², S. Kusch^{3,4}, A. L. Masterson², G.E. Lasher^{2,5}, M.R. Osburn²

Affiliations:

¹Department of Geology and Geophysics, University of Wyoming, Laramie, Wyoming

²Department of Earth and Planetary Sciences, Northwestern University, Evanston, Illinois

³Institut des sciences de la mer, Université du Québec à Rimouski, Rimouski, Canada

⁴CologneAMS—University of Cologne Centre for Accelerator Mass Spectrometry, University of Cologne, Cologne, Germany

⁵Department of Geology and Environmental Science, University of Pittsburgh, Pittsburgh, Pennsylvania

*jamie.mcfarlin@uwyo.edu

Summary

Arctic lakes are a major natural source of atmospheric methane (CH₄). Constraining future CH₄ emissions from Arctic lakes requires accounting for carbon-climate feedbacks that result from sustained warming^{1,2}. Sedimentary archives of past warm periods can reveal long-term carbon-climate feedbacks that are not fully apparent in modern observations. However, past lake CH₄ cycling is challenging to reconstruct³ and thus largely missing from the paleoenvironmental record. Here, we present the first evidence that the stable isotopic composition of hydrogen in sedimentary plant waxes from aquatic plants record changes in lake CH₄ dynamics, although the exact mechanism remains uncertain. We infer changes in Holocene lake CH₄ dynamics using changes in the H and C isotopic composition of these biomarkers in four widespread lakes across Greenland. In three of these lakes, we document increased uptake of CH₄ in aquatic plants for thousands of years during middle Holocene warming. Molecular biomarker and macrofossil abundances support that Holocene changes in CH₄ cycling were tightly related to local productivity and hypolimnetic oxygen. These Holocene data portend that ongoing warming of the Arctic will drive long-lasting physical and biological changes that may alter CH₄ cycling in many Greenland lakes and Arctic lakes more broadly.

Abstract

Methane (CH₄) emissions from Arctic lakes are of global concern in a warming world. Past Holocene warming provides an opportunity to examine carbon-climate feedbacks that develop over hundreds to thousands of years, but thus far records of past long-term changes in lake CH₄ dynamics are rare. Here, we demonstrate for the first time that the hydrogen stable isotopic composition of aquatic plant wax records incorporation of CH₄ in plant (aquatic moss) biomass. Trends in $\delta^2\text{H}$ and $\delta^{13}\text{C}$ values of aquatic plant derived leaf waxes point to widespread and sustained middle Holocene shifts in CH₄ cycling at climatically diverse sites across Greenland during millennia of elevated summer temperatures. Independent proxies indicate concurrent increases in local primary productivity and decreases in hypolimnetic oxygen. These data portend that ongoing warming may promote an enduring shift towards conditions that enhance methanogenesis in many Arctic lakes, including in lakes where these conditions do not exist today. This work highlights a previously unrecognized factor influencing $\delta^2\text{H}$ values of aquatic leaf waxes in some high-latitude lakes, and also draws attention to the role of common aquatic mosses as a potentially important sink of lake CH₄ across the Arctic that has yet to be quantified.

Main Text

Lakes are a significant natural source of the potent greenhouse gas methane (CH₄)¹. Arctic and boreal landscapes are warming faster than any other region on Earth² and have the highest density of lakes in the world⁴. CH₄ dynamics in high latitude lakes are sensitive to temperature^{1,5} and warming-driven feedbacks are expected to augment CH₄ emissions over the coming century^{1,6,7}. However, forecasting these emissions remains challenging⁸. Incomplete accounting for increased CH₄ from Arctic lakes contributes to the substantial uncertainty in projecting the global radiative budget over the coming century².

Geologic records of insolation-driven Arctic warmth and its consequences in the early to middle Holocene (11,700 to 4,200 years ago) provide unique opportunities to observe long-term shifts in lake systems in response to past sustained warming. The contributions from Arctic lakes to the Holocene CH₄ budget are poorly delineated relative to those from tropical and boreal wetlands^{9,10}. The C and H isotopic compositions of atmospheric CH₄ preserved in ice cores suggest that emissions from Arctic lakes increased during the middle Holocene, despite overall low global CH₄ emissions^{10,11}. However, Holocene CH₄ dynamics in northern lakes are not well-constrained^{3,12,13} thus limited support is available to test this hypothesis. Here, we present evidence that the stable isotopic compositions of aquatic plant waxes in Greenland lakes were strongly influenced by uptake of CH₄ during the middle Holocene. This finding indicates major middle Holocene changes in CH₄ dynamics in lakes across Greenland, particularly during

the summer when aquatic mosses grow the most. Although H isotopes in plant waxes are best known as a proxy with strong empirical relationships to meteoric water¹⁴, downcore H isotope values at several widespread sites presented here are too depleted to be derived from shifts in H isotopes of environmental water alone, requiring a strongly ²H-depleted input to explain the observed values. Independent evidence from lake sediments supports that this source is methane, which we hypothesize may be incorporated into plant wax through a symbiosis between aquatic mosses and methanotrophic microbes in low oxygen settings^{15,16}. Our evidence suggests that CH₄-derived H overprints the isotopic signal from lake water in these biomarkers during the middle Holocene at multiple sites on Greenland, making aquatic leaf wax $\delta^2\text{H}$ values at these sites an unreliable proxy for overall $\delta^2\text{H}_{\text{lakewater}}$ values but a novel indicator of changing CH₄ dynamics.

Plant wax is composed of *n*-alkyl lipids that are broadly source-specific by carbon chain-length, with mid-chain (*n*-C₂₀-C₂₅) compounds dominant in aquatic and non-vascular plant wax and long-chain (*n*-C₂₆₊) compounds most abundant in terrestrial and vascular plant wax¹⁷. These compounds are well preserved in sedimentary records on geologic time scales that range from hundreds of thousands to millions of years¹⁸. Waxes extracted from both modern plants and sediments demonstrate that the H isotope values ($\delta^2\text{H}$) of these compounds relate to $\delta^2\text{H}$ values of local meteoric water on a global scale, including at Arctic sites^{14,18}. This relationship occurs because plant intracellular water derived from local precipitation is predictably modified during lipid biosynthesis, producing waxes that are consistently ²H-depleted relative to growth water by ~100-150‰ depending on the plant type, compound, and growth conditions^{14,18}. This widely documented observation provides the basis for reconstructing local precipitation isotopes from sedimentary plant waxes through time.

Here, we reconstruct plant growth-water isotopes using biomarker isotope data from aquatic and terrestrial plants in four nonglacial lakes on Greenland spanning ~15° of latitude (Fig. 1). To do this, we present new Holocene wax H isotope records from Wax Lips Lake (WLL)¹⁹ and Trifna Sø (TS)²⁰ and revisit data previously published from Lake N3 (N3)^{21,22} and Pluto Lake (PL)^{22,23}. Detailed core descriptions and chronologies have been previously published for all lakes^{19–23}. The lakes in this compilation are small (<1 km²), through-flowing, and have been isolated from glacial meltwater since their deglaciation in the early Holocene, except for a brief discrete glacial period in the late Holocene at WLL¹⁹. Aquatic brown mosses (Class: Bryopsida, Family: Amblystegiaceae) are the major vegetation in many Arctic lakes²⁴ including the lakes presented here: Macrofossils of aquatic brown mosses (e.g., *Warnstorfia*, *Scorpidium*) are abundant in the sediment cores from these sites and today these plants form dense mats on the sediment surfaces^{19–22}. We estimate past $\delta^2\text{H}$ values of precipitation ($\delta^2\text{H}_{\text{precip}}$) using $\delta^2\text{H}$ values of long-chain sedimentary waxes (C₂₈-C₂₉; sourced from terrestrial plants), calibrated for plant

wax-water fractionation during wax synthesis using global average apparent fractionation factors ($\epsilon_{\text{app}} = -121 \pm 18\text{‰}$ for alkanes, $-99 \pm 32\text{‰}$ for acids)¹⁴. We reconstruct $\delta^2\text{H}$ values of aquatic moss growth water ($\delta^2\text{H}_{\text{moss}}$) using $\delta^2\text{H}$ values of mid-chain sedimentary waxes ($\text{C}_{21}\text{-C}_{24}$, sourced from aquatic plants), calibrated for plant wax-water fractionation using the same constant ϵ_{app} factors as for long-chain waxes stated above¹⁴ (Methods). While the error on each fractionation factor is quite large ($\pm 18\text{-}32\text{‰}$), the magnitude of change in H isotopes of mid-chain waxes at WLL, TS, and N3 far exceeds the range in error (Fig. 2). The observed magnitude of ^2H -depletion in $\delta^2\text{H}_{\text{moss}}$ values in the middle Holocene at TS, WLL, and N3 requires a distinct source of extremely ^2H -depleted H that can be integrated directly into mid-chain plant waxes but that does not affect long-chain waxes at these sites.

Holocene Precipitation Isotopes Across Greenland

We find, in agreement with prior publications, that terrestrial plant waxes at TS, N3, and PL become gradually more depleted through the Holocene (Fig. 2A, C, D), following multi-millennial trends similar to those of elevation-corrected oxygen isotope values from the Agassiz and Renland ice caps ($\delta^{18}\text{O}_{\text{ice}}$; Fig. 2F)^{25,26}, and reflect regional precipitation isotopes at each site. WLL terrestrial plant waxes show anomalous enrichment during the late Holocene compared with ice cores and terrestrial plant waxes at all other study lakes (Fig. 2B). Given that relatively enriched $\delta^2\text{H}_{\text{precip}}$ values in the late Holocene are not apparent in any other water isotope record from Greenland, including from nearby Agassiz, the late Holocene trend at WLL likely resulted from a localized change in the origin of plant waxes (e.g., increased representation of aeri ally transported waxes from lower latitudes)¹⁴ and/or a major change in terrestrial plant growing conditions (e.g., cold summer temperatures, strong aridity), rather than a change in isotopes of precipitation²⁷. The strongest amplitude of change in $\delta^2\text{H}_{\text{precip}}$ values occurs at the northernmost site TS with lower amplitude trends at N3 and PL. The diminishing amplitude of change in $\delta^2\text{H}_{\text{precip}}$ values by latitude is consistent with Holocene temperature reconstructions across Greenland, which show the strongest summer warming (up to $\sim +5^\circ\text{C}$ relative to modern averages) in the northernmost regions (Fig. 2E)^{19,28}.

H Isotopes of Aquatic Plants Decouple from Precipitation Isotopes at TS, WLL, and N3 during the Middle Holocene

The $\delta^2\text{H}_{\text{moss}}$ values at TS, WLL, and N3 are exceptionally ^2H -depleted in the early-middle Holocene relative to reconstructed $\delta^2\text{H}_{\text{precip}}$ values (Fig. 2A-C). The exact timing and duration of this depletion varies between TS and N3 ($\sim 7.5 - 3$ ka) and WLL ($\sim 10 - 2.5$ ka), but at all three sites, extremely depleted

$\delta^2\text{H}_{\text{moss}}$ values persist for thousands of years before a shift towards agreement with $\delta^2\text{H}_{\text{precip}}$ values in the late Holocene. Importantly, middle Holocene trends in $\delta^2\text{H}_{\text{moss}}$ values at TS, WLL, and N3 cannot be explained by contemporaneous changes in $\delta^2\text{H}_{\text{precip}}$ values regionally or seasonally: There is no concurrent ^2H -depletion in terrestrial plant wax in any lake and moreover even winter precipitation at the highest latitude in Greenland is not ^2H -depleted enough to achieve the observed $\delta^2\text{H}_{\text{moss}}$ values^{29–31}. Expanding on the latter point, we find that $\delta^2\text{H}_{\text{moss}}$ values are more ^2H -depleted than wax-inferred $\delta^2\text{H}_{\text{precip}}$ values by up to $\sim 160\text{‰}$, $\sim 170\text{‰}$, and $\sim 180\text{‰}$ at TS, WLL, and N3 respectively. A mechanism invoked previously to explain divergent H isotope trends in mid- vs. long-chain plant waxes, including at N3, is changing seasonality of the precipitation stored in lakes, e.g., increased cold-season precipitation^{21,22,32}. However, modern seasonal extremes in precipitation $\delta^2\text{H}$ values at each site are too small to account for this change, only differing by $\sim 80\text{--}90\text{‰}$ at N3 and TS, and $\sim 130\text{‰}$ in the intensely seasonal climate at WLL (Fig. 2A–C)^{29–31}. We tested this quantitatively with an isotope mass balance model (Fig. 3; Methods), confirming that this mechanism cannot explain observed depletions in $\delta^2\text{H}_{\text{moss}}$ values at TS, WLL, and N3. This finding holds even when our model uses climatically improbable conditions (e.g., 100% input of the winter endmember, that is, the most depleted monthly average $\delta^2\text{H}$ value observed in modern precipitation, used for $\delta^2\text{H}_{\text{lakewater}}$ values) and when accounting for analytical uncertainties (i.e., 1σ variability of wax-water fractionation factor): modeled $\delta^2\text{H}_{\text{moss}}$ values are still at least $\sim 30\text{--}60\text{‰}$ more enriched than the most depleted observed $\delta^2\text{H}_{\text{moss}}$ values at TS and N3 (Fig. 3). As further evidence against a scenario of middle Holocene winter-dominated $\delta^2\text{H}_{\text{lakewater}}$ values in Greenland lakes, there is no concurrent signal of increased winter precipitation evident in $\delta^{18}\text{O}_{\text{ice}}$ values from nearby ice core sites which accumulate precipitation throughout the year. Instead, $\delta^{18}\text{O}_{\text{ice}}$ was least depleted in the early-middle Holocene (Fig. 2F)^{25,26}. Furthermore, the between-site similarity of depletion in $\delta^2\text{H}_{\text{moss}}$ values, especially between TS and N3, suggests a consistent mechanism, despite the distance between these sites and markedly different climate and precipitation regimes^{33,34}. We also ran more climatically probable models (given that mean annual modern precipitation is slightly summer-biased at all sites³⁴) using 50–75% input of winter endmember as $\delta^2\text{H}_{\text{lakewater}}$ values instead. These³⁴ yield discrepancies between $\delta^2\text{H}_{\text{moss}}$ values and those of wax-inferred $\delta^2\text{H}_{\text{precip}}$ values of $\sim 100\text{‰}$ at TS and N3 (Fig. 3).

In addition, independent reconstructions of Holocene lake water isotopes at WLL (new data) and N3 (published data)³² are available, based upon the oxygen isotopic composition of chitinous head capsules of obligate aquatic insect larvae (Chironomidae, $\delta^{18}\text{O}_{\text{chiron}}$; see Methods). These $\delta^{18}\text{O}_{\text{chiron}}$ -inferred lake water $\delta^{18}\text{O}$ reconstructions strongly agree with wax-inferred $\delta^2\text{H}_{\text{precip}}$ values from long-chain, terrestrial plant waxes at the same lakes (Fig. 2B, C) and, unlike $\delta^2\text{H}_{\text{moss}}$ values, neither demonstrates any

depletion during the middle Holocene. Chironomid larvae in Arctic lakes live for multiple years and may grow year-round³⁵. Analyses from lakes around the world, including Greenland, and from laboratory cultures show that $\delta^{18}\text{O}_{\text{chiron}}$ values are strongly controlled by $\delta^{18}\text{O}_{\text{water}}$ values^{36,37}. Chironomid $\delta^{18}\text{O}$ values thus provide an independent estimate of the isotopic composition of average lake water to compare against $\delta^2\text{H}_{\text{moss}}$ and $\delta^2\text{H}_{\text{precip}}$ values derived from plant waxes; these show no depletion in water during the middle Holocene at the two sites where $\delta^{18}\text{O}_{\text{chiron}}$ was measured, WLL and N3. In summary, diverse lines of evidence indicate that $\delta^2\text{H}_{\text{moss}}$ values cannot be explained by changes in the isotopes of local meteoric water during the Holocene and another explanation for extremely light $\delta^2\text{H}_{\text{moss}}$ values in the middle Holocene is required. We argue below that incorporation of isotopically light H from CH_4 is the only viable explanation and is supported by diverse independent evidence.

Evidence for Changes in Methane Cycling at TS

Independent proxy evidence from TS in northeast Greenland indicates both high carbon loading and low hypolimnetic oxygen during the period of depleted $\delta^2\text{H}_{\text{moss}}$ values from ~4 to 8 ka (Fig. 4)²⁰. The ratio of isoprenoidal GDGT-0: crenarchaeol increased, supporting strong archaeal methanogenesis^{38,39}, as did the fractional abundance of bacterial branched GDGT-IIIa⁴⁰ implying a drop in O_2 (Fig. 4C, D). The middle Holocene low in hypolimnetic oxygen and peak in archaeal methanogenesis at TS was accompanied by elevated aquatic invertebrate and terrestrial plant macrofossil abundances, indicating a rise in local productivity both within and around the lake and consequently greater supply of organic carbon to sediments (Fig. 4E, F)²⁰. Trends in $\delta^2\text{H}_{\text{moss}}$ values are highly anti-correlated ($r = -0.7$ to -0.8 , $p < 0.001$) to the trends in these sedimentary indicators but are not related to trends in wax-inferred $\delta^2\text{H}_{\text{precip}}$ values (Extended Data Fig. S1).

Further, at TS the carbon isotopic composition of sedimentary moss waxes (C_{21} and C_{23} $\delta^{13}\text{C}_{\text{wax}}$ values; average analytical error of $1\sigma = 0.15\text{‰}$ VPDB) demonstrate a strong relative ^{13}C -depletion concurrent with the ^2H -depletion in $\delta^2\text{H}_{\text{moss}}$ values (Fig. 4B) that is not apparent in terrestrial waxes (Extended Data Fig. S2). A symbiotic relationship between both *Sphagnum* (Class: Sphagnopsida, Family: Sphagnaceae) and brown mosses and methanotrophic bacteria is well-documented^{15,16,41}. Moss-associated methane-oxidizing bacteria (MAMO) form dense colonies within moss cells and on moss surfaces¹⁶, where they oxidize CH_4 using O_2 produced during photosynthesis, and in turn provide the moss CO_2 and H_2O ^{15,16,42,43}. Data from Siberian ponds has demonstrated that 60-99% of the CH_4 produced by sedimentary methanogens in anoxic ponds is oxidized within aquatic brown moss layers,⁴⁴ demonstrating MAMO are highly efficient at consuming CH_4 in the water column. Other recent studies

show substantial rapid uptake of CH₄ and N₂ in submerged mosses with methanotrophic symbionts⁴⁵. Short-term culturing experiments documenting this symbiosis using ¹³C-labelled CH₄ have shown that conservatively 30% to 40% of C in new biomass in *Sphagnum* and *Scorpidium*, respectively, is derived from CH₄^{15,16}. CH₄-derived C is most strongly incorporated in submerged mosses (compared to non-submerged mosses) regardless of the species^{15,42,43,46}. Using a C isotope mass balance model, we estimate that during the middle Holocene up to ~25% of the C in aquatic moss waxes at TS was derived from CH₄ (Extended Data Fig. S3; Methods), consistent with culturing studies^{15,16}. This observation supports both 1) that a change in CH₄ cycling occurred at TS specifically during the warm-season months when aquatic mosses generate most of their biomass^{24,47,48} and 2) that CH₄-oxidation products including CO₂ were available to aquatic mosses during the middle Holocene. Uptake of CH₄-derived C also provides an intriguing explanation for the strong ¹⁴C-depletion observed for moss fossils in both TS and neighboring Sneha Sø, which thus far had to be explained by reworking^{20,49}.

To our knowledge, no study has examined if CH₄-derived H from MAMO is incorporated into moss biomass, but our findings point to a need for future work in this area. Because lacustrine CH₄ is substantially ²H-depleted relative to meteoric water due to strong discrimination against heavy isotopes during methanogenesis (e.g., ~ -250‰ relative to growth water in Arctic wetlands)^{50,51}, any CH₄-derived H in products yielded during methane oxidation (e.g., H₂O, NH₄⁺)⁴⁵ that enter the intracellular H pool of mosses are likely to significantly influence the H isotopic composition of synthesized biomass¹⁸. We find that when tested in an isotope mass balance model, δ²H_{moss} values at WLL, TS and N3 all require the input of H derived from CH₄ to achieve the magnitude of ²H-depletion observed during the middle Holocene (Extended Data Fig. S3; Methods). Using wax-inferred δ²H_{precip} values as a baseline for the isotopic composition of contemporaneous lake water at TS, our isotope mass-balance model demonstrates that up to ~80% of H in aquatic moss waxes at TS comes from CH₄. We note that this is a much higher proportion of CH₄ than modeled for C and the specific mechanism for this imbalance remains unclear. One possible explanation may reside in the metabolic pathway used by MAMO. Limited ¹³C-depletion of bacterial biomarkers (-31 to -38‰, in good agreement with our observations) has been demonstrated in *Sphagnum*-associated Type II methane oxidizing bacteria (MOB), which use the serine carbon fixation pathway and assimilate CO₂ in addition to CH₄⁵². Moreover, δ¹³C values in biomarkers from MOB also seem to depend on the ambient temperature, with lower temperatures muting ¹³C-fractionation⁵³. Accordingly, the relative amount of MAMO-derived CH₄-C in the total fixed C pool may be reduced. Regardless, it appears that MAMO is an unexplored source of ²H-depletion in sedimentary wax isotopes which are widely applied to Arctic lakes.

Middle Holocene Changes to CH₄ Cycling on Greenland

Three of the four lakes examined here (TS, WLL, and N3) require the incorporation of CH₄-derived H into moss waxes to fully explain $\delta^2\text{H}_{\text{moss}}$ values during the middle Holocene. That the fourth lake (PL) does not show extremely depleted $\delta^2\text{H}_{\text{moss}}$ values or (therefore) appears to not record moss-associated methane oxidation, is consistent with its vegetation and lake bathymetry. Specifically, only the lakes with moss reported as an abundant constituent in core material and with geometries more prone to thermal stratification in the summer demonstrate uptake of CH₄-derived H in $\delta^2\text{H}_{\text{moss}}$ values. CH₄ production and storage in northern lakes is controlled seasonally by different mechanisms: while many lakes become anoxic during the Arctic winter due to ice cover⁵⁴, in relatively deep lakes with small surface areas (< 1 km²) and high nutrient loads, CH₄ concentrations can also increase in the hypolimnion during ice-free summer months when lakes are thermally stratified and thus O₂ limited^{55,56}. Shallow lakes and those with larger surface areas, which promotes wind-driven mixing, in contrast are less likely to stratify in the summer. The thickness of the hypolimnion in summer-stratified Arctic lakes increases when light penetration depth decreases as lakes become more productive⁵⁷, and additionally increases with higher water temperatures and longer ice-free seasons which strengthen thermal stratification^{56–58}. Aquatic moss growth has been shown to strongly favor hypolimnetic water of summer-stratified lakes⁴⁸ and moss photosynthesis is mostly light- and nutrient-limited in the Arctic winter, therefore MAMO are likely to thrive during the open-water season in stratified lakes^{24,47,48}. These requisites predict which lakes in our dataset will preserve CH₄-derived H in moss biomarkers during the middle Holocene (TS, WLL, and N3, with maximum water depths of ~6, 9, and 16 m respectively and abundant moss noted in sediment cores), and which lakes do not (PL, the shallowest lake in this dataset, with water depth of ≤4m).

Implications for the Impact of Past and Future Warming

Precipitation isotopes at all sites, as inferred from $\delta^2\text{H}$ values of long-chain terrestrial plant waxes, parallel multi-millennial trends in ice cores and follow the broad, insolation-driven pattern of long-term cooling through the Holocene. Although peak summer warmth occurred in the early Holocene across much of Greenland (see Fig. 2E), summer temperatures remained elevated above those of the 20th century through the middle Holocene. Primary production at many sites peaked during the warm middle Holocene following several millennia of post-glacial ecosystem succession and watershed evolution^{28,59}. We find that the middle Holocene combination of warmth and elevated primary production, as previously inferred from aquatic and terrestrial macrofossil abundances at TS, was accompanied by major shifts in lake CH₄ cycling in multiple sectors of Greenland as evident in $\delta^2\text{H}_{\text{moss}}$ values at WLL, TS and N3. That

$\delta^2\text{H}_{\text{wax}}$ values of aquatic plants appear to integrate H from CH_4 is a new observation, presenting a paradigm shift for interpreting $\delta^2\text{H}_{\text{wax}}$ records from lakes across the Arctic. Mechanistically, we postulate 1) that a combination of higher summer air and water temperatures and the attendant longer ice-free seasons paired with greater primary production contributed to more persistent summer stratification of TS, WLL, and N3 during the middle Holocene, when solubility of O_2 was also lower and delivery of nutrients and organic matter to lakes was higher, and 2) that these redox conditions promoted methanogenesis, increased CH_4 cycling in the hypolimnion, and favored MAMO (Extended Data Fig. S4). The major shifts in lake CH_4 dynamics at TS, WLL, and N3 occurred during a period of only +1-3°C summer warming relative to the 20th century but followed a prolonged early Holocene period of warming and watershed ontogeny after regional deglaciation.

Strong incorporation of CH_4 -derived H into aquatic moss biomass at TS, WLL, and N3 during the middle Holocene demonstrates that CH_4 dynamics drastically changed in widespread lakes for thousands of years during the last period of prolonged relative warmth and greening across Greenland. Elevated methanogenesis in these Arctic lakes occurred when global CH_4 production was at a Holocene low and may help explain why CH_4 emissions decreased more strongly in the tropics than the Arctic in the middle Holocene, despite a reduction in methanogenesis from boreal peatlands¹¹. Incorporation of CH_4 -derived H into aquatic moss biomass, and thus inferred warm-season methanogenesis, decreased at all three affected study sites with summer cooling of ~1-3°C in the late Holocene, revealing an important climate dependence on Arctic lake CH_4 cycling. This paleolimnological perspective from a suite of widespread and climatically diverse Greenland lakes suggests that ongoing warming and extension of the ice-free season, paired with predicted increases in primary production, will drive increases in lake CH_4 production in lakes across Greenland and the Arctic and thus higher emissions potential over the coming decades to centuries. In many of these high-latitude lakes, our results also suggest that the widespread presence of aquatic mosses may act as a quantitatively important sink for CH_4 —pointing to a complex role for Arctic lakes in the future global carbon cycle. The incorporation of CH_4 -derived H into plant biomass offers a means for reconstructing how lake redox conditions and carbon cycling changed during past periods of warmth.

Methods

Sedimentary Wax Concentration, and Hydrogen and Carbon Isotopic Composition

Trifna Sø (TS) sediment cores are thoroughly described by Kusch et al. (2019), including sediment storage, preparation, and lipid and macrofossil extraction and analyses²⁰. Wax Lips Lake (WLL) sediment

cores are thoroughly described in McFarlin et al. (2018)¹⁹. For biomarker work, WLL cores were refrigerated at 4°C for ~1 year prior to subsampling for biomarker analyses. Lipids were extracted from 0.5-3 g of lyophilized sediment using a MARS Microwave ExtractorTM in 20 ml of 9:1 DCM: MeOH. The extraction program included a 5-minute ramp to 100°C, 20 minutes at 100°C, and a minimum of 30-minute cool down period. Total lipid extracts (TLEs) were filtered and saponified in 0.5 NaOH at 70°C for 8-12 hours, then acidified and separated from the aqueous phase using methyl-tert-butyl ether (MTBE) 3x. TLEs were then separated into fractions (alkanes, alcohols, acids) using Discovery (Sigma Aldrich) amino-propyl solid phase extraction (SPE) columns sequentially eluting with hexane, 9:1 DCM: acetone, 2.5% formate in DCM respectively. Saturated alkanes were separated from unsaturated alkanes using Discovery (Sigma Aldrich) Ag-ion SPE columns, eluting with hexane and acetone respectively.

WLL alkanes were quantified via gas chromatography using a Thermo Scientific Trace 1310 gas chromatograph (GC) with a ZB5 30 m x 0.25 mm ID x 0.25 µm film thickness (Zebron) column coupled to Flame Ionization Detector (FID) and a Thermo DSQ single quadrupole mass spectrometer. The GC program used for quantification ramped oven temperatures at 6°C/minute from 100°C to 330°C. Alkanes were identified via diagnostic mass spectra, comparison to the NIST and in-house libraries, and retention times relative to laboratory standard compounds. Concentrations were calculated from FID peak areas through comparison to that of a 10 µg palmitic acid isobutyl ester (PAIBE) internal quantification standard.

Compound specific carbon (¹³C/¹²C) and hydrogen (²H/¹H) isotopic analyses on alkanes for TS and/or WLL were conducted via GC isotope ratio mass-spectrometry (GC-IRMS) using a Thermo Scientific Trace GC with a ZB5-5MS 30 m x 0.25 mm ID x 1 µm film thickness column coupled to a Thermo Delta V Plus IRMS via a pyrolysis (P) or combustion (C) interface and controlled by a Thermo GC-C III via Isodat. Reactions for GC-Pyrolysis-Compound Specific Isotope Analysis (GC-P-CSIA) occurred in an alumina column held at 1420°C with a flow of 1.4 mL/min. Reactions for GC-Combustion-CSIA (GC-C-CSIA) occurred in an oxidizing reactor consisting of a 2XCu/Ni/Pt 0.1 m wire bundle held at 940°C. Tank calibration to the VSMOW and VPDB-LSVEC scales utilized a C₁₆-C₃₀ *n*-alkane standard (A6, Arndt Schimmelmann, Indiana University) and a derivatized C₁₄-C₂₀ fatty acid methyl ester (FAME) mixed standard (F8b, Alex Sessions, Caltech). Instrumental error was assessed via root mean standard error (RMSE) on F8 and A6, which was run between every 3 sample duplicates and averages <5‰ (alkanes). The H₃⁺ factor was determined and applied regularly and averaged 5.214 ppm/nA during the analytical period during 2016 when WLL samples were run and averaged 3.394 ppm/nA during the analytical period during 2019 when TS samples were run. For each sample, the alkane fractions were measured in duplicate for ²H/¹H- and ¹³C/¹²C-isotope analyses. Compound-specific δ²H

and $\delta^{13}\text{C}$ values are reported as average duplicate values on the VSMOW and VPDB-LSVEC scale respectively. Total analytical error presented on $\delta^2\text{H}$ and $\delta^{13}\text{C}$ values includes the 1σ of measurements on each compound peak as well as the instrumental error over the course of all sample measurements, propagated using the root sum of squares (RSS). $\delta^{13}\text{C}$ values of FAMEs were corrected for the addition of the methyl group during derivatization via a derivatized phthalic acid of known C isotopic composition.

Oxygen isotopic composition of chironomid head capsules

Wax Lips Lake (WLL) sediment samples of 4 to 8 ccs (representing 2 cm of core depth) were collected for chironomid $\delta^{18}\text{O}$ analysis. Each sample was deflocculated in a 10% KOH solution at 20°C for 30 minutes, then sieved in DI water using 150 μm mesh. Chironomid head capsules were manually picked and cleaned of any remaining adhering material under a dissecting microscope, then transferred to oven dried 3.2 x 4 mm lightweight Elemental Microanalysis® silver capsules. On average, ~100 head capsules were collected for each analysis (totaling ~100 μg analyte material). The filled silver capsules were thoroughly freeze dried and analyzed for $\delta^{18}\text{O}$ values on a Thermo Scientific™ High Temperature Conversion Elemental Analyzer (TC/EA) coupled to a Thermo Scientific™ Delta V Isotope Ratio Mass Spectrometer (IRMS) via a Conflo IV interface in the Northwestern University Stable Isotope Laboratory. The TC/EA pyrolysis was conducted at 1450°C and standardization to the VSMOW scale was done via calibration with a mixture of organic (e.g., benzoic acid) and inorganic (e.g., BaSO_4) standards including benzoic acid #A (Indiana University) and NBS127, IAEA-SO5, IAEA-SO6. Average precision on standards during the analytical period was $\pm 0.4\text{‰}$. Original chironomid $\delta^{18}\text{O}$ values are reported as per mil (‰) relative to VSMOW.

A downcore subset of isolated chironomid remains were also checked for the presence of carbonates using Fourier Transform Infrared Spectroscopy (FT-IR). Individual head capsules were scanned on a Bruker Hyperion 2000 series FT-IR Microscope system between 600 and 4000 cm^{-1} at 32 times per 4 cm^{-1} resolution. Peaks characteristic of carbonate at ~ 712 , ~ 862 and $\sim 1440\text{ cm}^{-1}$ (corresponding to the in-plane bending vibration, the out-of-plane bending vibration and the asymmetric stretching of bonds in a CO_3^{2-} molecule^{60–62}) were not present in the spectra of any samples.

Analysis of downcore chironomid $\delta^{18}\text{O}$ values were attempted for TS but not enough chironomid material remained to perform isotope measurements. Unfortunately, chironomid samples originally prepared by Kusch et al. (2019) were not archived.

Correction of H wax and O chironomid isotope values to water isotope values

The $\delta^2\text{H}$ values of plant wax alkanes and acids are calibrated to water $\delta^2\text{H}$ values using the global average apparent fractionation factor estimated from $n\text{-C}_{29}$ alkanes ($\epsilon_{\text{app}} = -121 \pm 18\text{‰}$) and $n\text{-C}_{28}$ alkanic acids ($\epsilon_{\text{app}} = -99 \pm 32\text{‰}$) respectively from McFarlin et al. (2019)¹⁴. The 1σ error on each calibration is represented with error bars in the upper right corner in Figure 2A-D. These calibrations are estimated from sedimentary long-chain waxes but applied to both mid- and long-chain compounds here because there is existing precedent in the wax literature to assume wax-water fractionation factors of aquatic plants are equal to that of terrestrial plants^{21,22,63–65}. This precedent is supported by the available observations of wax-water fractionation factors in sedimentary waxes which show statistically indistinguishable fractionation factors between mid-chain waxes and lake water ($\epsilon_{\text{app}} = -121 \pm 50\text{‰}$, $n=46$ for $n\text{-C}_{23}$ alkanes and $\epsilon_{\text{app}} = -112 \pm 33\text{‰}$, $n=109$ for $n\text{-C}_{24}$ alkanic acids in global data compiled by McFarlin et al. (2019)) compared to long-chain waxes and precipitation, albeit with substantially fewer observations of the former¹⁴. This precedent is also supported by agreement within error of the apparent fractionation values observed in modern aquatic and non-vascular plants^{14,66–68}. While larger fractionation effects have been observed in some aquatic plants growing in saline water or heterotrophically in dark conditions^{69,70}, neither of these parameters are consistent with aquatic moss growth during the Arctic summer in non-glacial freshwater lakes^{24,48}.

The $\delta^{18}\text{O}$ values of chironomid head capsules are converted to $\delta^{18}\text{O}_{\text{lakewater}}$ values using a regression from Van Hardenbroek et al. (2018) (Equation 1) with residual standard error on this estimate of 2.4‰ ³⁶. $\delta^2\text{H}_{\text{WLL}}$ values are estimated from $\delta^{18}\text{O}_{\text{lakewater}}$ values using the local meteoric water line (LMWL) which is constrained using observations recorded in the IAEA-GNIP database from the nearby Pituffuk Station (Thule, ~60 km from WLL) (Equation 2)³⁰, with residual standard error on this relationship of 9‰ . $\delta^2\text{H}_{\text{N3}}$ values are estimated from $\delta^{18}\text{O}_{\text{lakewater}}$ values using the LMWL for western Greenland reported by Corcoran et al. (2021) (Equation 3)³². The error on chironomid-estimated $\delta^2\text{H}_{\text{lakewater}}$ values represented in Fig. 2 for WLL and N3 is the compounded error that includes the analytical error on the oxygen isotope measurements of chironomids ($\pm 0.4\text{‰}$ for WLL and $\pm 0.2\text{‰}$ for N3)³², residual standard error on the Van Hardenbroek et al. (2018) regression ($\pm 2.4\text{‰}$)³⁶, both of which are propagated during O to H isotope calculations, and residual standard error on the LMWL ($\pm 9\text{‰}$, estimated using the LWML from WLL).

$$\delta^{18}\text{O}_{\text{lakewater}} (\text{‰VSMOW}) = (0.96 * \delta^{18}\text{O}_{\text{chiron}}) - 22.6 \text{ (Equation 1)}$$

$$\delta^2\text{H}_{\text{WLL}} (\text{‰VSMOW}) = (7.33 * \delta^{18}\text{O}_{\text{lakewater}}) - 7.1 \text{ (Equation 2)}$$

$$\delta^2\text{H}_{\text{N3}} (\text{‰VSMOW}) = (6.8 * \delta^{18}\text{O}_{\text{lakewater}}) - 13.7 \text{ (Equation 3)}$$

Water H isotope mass-balance model for TS, WLL, and N3

We assume that $\delta^2\text{H}_{\text{precip}}$ values, estimated from $\delta^2\text{H}$ values of long-chain plant waxes ($n\text{-C}_{29}$ alkanes at TS, WLL; $n\text{-C}_{28}$ acids at N3), are representative of the growth water available to terrestrial plants during the summer growing season at each site and that this precipitation will also enter the lake. $\delta^2\text{H}_{\text{precip}}$ values therefore provide one input to lake water at each site and can be used to assess if endmember $\delta^2\text{H}_{\text{winter}}$ values (i.e., the most depleted winter precipitation isotopes observed in modern monthly data, estimated at -190‰, -220‰, and -260‰ at N3, TS, and WLL respectively)^{29,31} can fully explain the observed $\delta^2\text{H}_{\text{mooss}}$ values at their most depleted point in the middle Holocene (Equation 4). We assume that where $\delta^2\text{H}_{\text{mooss}}$ values are their most depleted relative to $\delta^2\text{H}_{\text{precip}}$ values (ϵ_{max}) during the middle Holocene represents when moss growth water (i.e., $\delta^2\text{H}_{\text{lake}}$) would have been most weighted towards winter precipitation if this were indeed the mechanism driving trends in $\delta^2\text{H}_{\text{mooss}}$ values at each site and allow the models to incorporate 100% endmember $\delta^2\text{H}_{\text{winter}}$ values for $\delta^2\text{H}_{\text{lake}}$ (0% wax-inferred $\delta^2\text{H}_{\text{precip}}$ values) at this point in time for each record. We then scale the input of endmember $\delta^2\text{H}_{\text{winter}}$ values at all other points in time relative to this point based on the epsilon value between mid- and long-chain wax $\delta^2\text{H}$ values ($\epsilon_{\text{terr-aq}}$) (Equation 5) given the assumption being tested here that differences in $\epsilon_{\text{terr-aq}}$ throughout the Holocene are a function of the amount of winter input to each lake.

$$\delta^2\text{H}_{\text{lake}} (\text{‰VSMOW}) = (n) * \delta^2\text{H}_{\text{winter}} + (1-n) * \delta^2\text{H}_{\text{precip}} \text{ (Equation 4)}$$

$$n = \epsilon_{\text{terr-aq}} / \epsilon_{\text{max}} \text{ (Equation 5)}$$

Due to the uncertainty in the apparent fractionation factor used to calibrate $\delta^2\text{H}_{\text{wax}}$ values to $\delta^2\text{H}_{\text{precip}}$ or $\delta^2\text{H}_{\text{mooss}}$ values we also allow for a 1 σ error in these estimates, which is represented in Figure 3. Because there is no incorporation of $\delta^2\text{H}_{\text{precip}}$ values at the point when $\delta^2\text{H}_{\text{mooss}}$ values are the most depleted, the estimates of wax-inferred $\delta^2\text{H}_{\text{precip}}$ values are somewhat irrelevant to testing if any amount of winter precipitation can fully explain depleted $\delta^2\text{H}_{\text{mooss}}$ values. We find that 100% winter endmember precipitation cannot explain $\delta^2\text{H}_{\text{mooss}}$ values at TS or N3 during the middle Holocene, and that 100% winter endmember precipitation can only just explain the early to middle Holocene trends at WLL if we apply the largest fractionation factor in our range ($\epsilon_{\text{app}} = -139\text{‰}$). However, full incorporation of only an

extreme winter endmember is climatically improbable (e.g., even an average of winter precipitation across all winter months would be substantially less depleted than the winter endmember) and we have also included models that set the maximum uptake of winter endmember precipitation at 75% and 50% (Equation 6, 7).

$$n_{75} = 0.75 * (\epsilon_{\text{terr-aq}} / \epsilon_{\text{max}}) \text{ (Equation 6)}$$

$$n_{50} = 0.50 * (\epsilon_{\text{terr-aq}} / \epsilon_{\text{max}}) \text{ (Equation 7)}$$

These latter models are more climatically probable and yield lake water values that are in closer agreement with the H isotopic composition of mean annual precipitation at each site^{27,28,66}. We note that modern lake water $\delta^2\text{H}$ values at both WLL (-153‰) and N3 (-96‰) are currently strongly summer-biased, suggesting very little retention of any winter precipitation in lake water into the summer months at these sites at present. We unfortunately have no measurements of modern lake water isotopes for TS. The $\delta^2\text{H}_{\text{lake}}$ values that result from mixing of the two precipitation endmembers we present here demonstrate the improbability that winter precipitation would ever dominate in these lakes, where equal or more precipitation amounts are delivered during the summer season³² and given the competing input of more enriched summer precipitation during the early-middle Holocene at each site.

CH₄-Isotope Mass Balance Model for TS

We posit that C and H derived from CH₄ provides an alternative source of exceptionally isotopically light H and C to aquatic plant wax. We estimate the amount of CH₄-derived H that is utilized during lipid biosynthesis by aquatic moss by using an isotope mass balance model that assumes $\delta^2\text{H}_{\text{moss}}$ values are a product of two endmembers: wax-inferred $\delta^2\text{H}_{\text{precip}}$ values and $\delta^2\text{H}_{\text{CH}_4}$ values as H-derived from CH₄. $\delta^2\text{H}_{\text{CH}_4}$ values are estimated through the Holocene at TS using the dataset from Chanton et al. (2006)⁵⁰ which demonstrates biogenic $\delta^2\text{H}_{\text{CH}_4}$ in high-latitude wetlands is ~ -250‰ relative to environmental water, with environmental water through the Holocene at TS estimated using wax-inferred $\delta^2\text{H}_{\text{precip}}$ values (Equation 8). The percent of CH₄-derived H represented in $\delta^2\text{H}_{\text{moss}}$ values is estimated using Equation 9.

$$\delta^2\text{H}_{\text{CH}_4} (\text{‰VSMOW}) = 1000 * (((1000 + \delta^2\text{H}_{\text{precip}}) / (1000 - (-250)) - 1) \text{ (Equation 8)}$$

$$\text{CH}_4\text{-H (\%)} = (\delta^2\text{H}_{\text{moss}} - \delta^2\text{H}_{\text{precip}}) / (\delta^2\text{H}_{\text{CH}_4} - \delta^2\text{H}_{\text{precip}}) \text{ (Equation 9)}$$

We estimate the amount of CH₄-derived C that is utilized during lipid biosynthesis by aquatic moss by using an isotope mass balance model that assumes $\delta^{13}\text{C}_{\text{moss}}$ values are a product of two endmembers: a baseline of $\delta^{13}\text{C}_{\text{CO}_2} = -30\text{‰}$ (VPDB) which represents the value of $\delta^{13}\text{C}_{\text{moss}}$ in the early Holocene, prior to the onset of depleted H isotope values in the middle Holocene and assume $\delta^{13}\text{C}_{\text{CH}_4} = -50\text{‰}$ (VPDB) as a conservative estimate based on modern environmental observations in several West Greenland lakes by Cadieux et al. (2016), which range from ~ -30 to -70‰ (VPDB)⁵⁶. The percent of CH₄-derived C represented in $\delta^{13}\text{C}_{\text{moss}}$ values at TS is estimated using Equation 10.

$$\text{CH}_4\text{-C (\%)} = (\delta^{13}\text{C}_{\text{moss}} - \delta^{13}\text{C}_{\text{CO}_2}) / (\delta^{13}\text{C}_{\text{CH}_4} - \delta^{13}\text{C}_{\text{CO}_2}) \text{ (Equation 10)}$$

CH₄-derived H₂O in intracellular water

Intracellular water in aquatic plants and mosses is sourced from lake water and it is thought that methanotrophic symbionts are able to colonize aquatic moss via water transport^{15,16}. It is therefore unlikely that the spaces in which MAMO reside are not freely exchanging H₂O. This presents a challenge for identifying the exact mechanism by which MAMO supplies CH₄-derived H to aquatic mosses in appreciable amounts. If it were limited to the H₂O produced during the oxidation of CH₄, the exchange of CH₄ would need to be 10⁵ to 10⁶ times more rapid than the exchange of water within the cell, given the molarity of lake water relative to the concentration of CH₄ even in lakes with elevated dissolved CH₄ ($\sim 100 \mu\text{M CH}_4/\text{L}$)⁵⁸. Prior work has shown that MAMO can oxidize $80 \mu\text{M CH}_4/\text{g dry plant mass/day}$ ⁴¹ and there exists speculation that aquatic mosses have unique carbon concentrating mechanisms given how slowly CO₂ diffuses in water and the inability of these plants to use bicarbonate⁷¹. However, to our knowledge, there is no work on aquatic brown mosses that can point to whether or not this mechanism alone is a sufficient explanation. Understanding of the source of H to NADPH pools and the cycling of NADPH in plants is limited but recognized as a major control on intracellular water and the H isotopic composition of plant lipids¹⁸. In this work, isotope mass balance demonstrates that the observed $\delta^2\text{H}_{\text{moss}}$ values at WLL, TS, and N3 can only be achieved by incorporating CH₄-derived H into moss lipids. However, understanding this relationship is outside the scope of this work and extensive future studies using modern observations in stratified and methane-producing Arctic lakes with aquatic moss, MAMO culturing experiments, and lipid stable isotope probing will likely be necessary to understand this system in full detail.

Data availability

All novel data [will be] publicly archived with NOAA/World Data Service for Paleoclimatology. R code and all data used in these analyses are also publicly available on Github at <https://github.com/JmMcFarlin/McFarlin-et-al-.git>. Any remaining lipid extracts for WLL and TS are housed at Northwestern University.

References

1. Wik, M., Varner, R. K., Anthony, K. W., MacIntyre, S. & Bastviken, D. Climate-sensitive northern lakes and ponds are critical components of methane release. *Nat Geosci* **9**, 99–105 (2016).
2. Collins, M. *et al.* 2013: Long-term Climate Change: Projections, Commitments and Irreversibility. in *Climate Change 2013: The Physical Science Basis. Contribution of Working Group I to the Fifth Assessment Report of the Intergovernmental Panel on Climate Change* 1029–1136 (Cambridge University Press, 2013).
3. Sundqvist, H. *et al.* Arctic Holocene proxy climate database—new approaches to assessing geochronological accuracy and encoding climate variables. *Climate of the Past* **10**, 1605–1631 (2014).
4. Verpoorter, C., Kutser, T., Seekell, D. A. & Tranvik, L. J. A global inventory of lakes based on high-resolution satellite imagery. *Geophys Res Lett* **41**, 6396–6402 (2014).
5. Wik, M. *et al.* Energy input is primary controller of methane bubbling in subarctic lakes. *Geophys Res Lett* **41**, 555–560 (2014).
6. Walter, K. M., Smith, L. C. & Chapin, F. S. Methane bubbling from northern lakes: Present and future contributions to the global methane budget. *Philosophical Transactions of the Royal Society A: Mathematical, Physical and Engineering Sciences* **365**, 1657–1676 (2007).
7. Walter, K. M., Zimov, S. A., Chanton, J. P., Verbyla, D. & Chapin, F. S. Methane bubbling from Siberian thaw lakes as a positive feedback to climate warming. *Nature* **443**, 71–75 (2006).
8. Engram, M. *et al.* Remote sensing northern lake methane ebullition. *Nat Clim Chang* **10**, 511–517 (2020).
9. Zheng, Y. *et al.* Holocene variations in peatland methane cycling associated with the Asian summer monsoon system. *Nat Commun* **5**, 4631 (2014).
10. Zheng, Y. *et al.* Operation of the boreal peatland methane cycle across the past 16 k.y. *Geology* **48**, 82–86 (2020).
11. Sowers, T. Atmospheric methane isotope records covering the Holocene period. *Quat Sci Rev* **29**, 213–221 (2010).
12. Elvert, M. *et al.* Methane turnover and environmental change from Holocene lipid biomarker records in a thermokarst lake in Arctic Alaska. *Holocene* **26**, 1766–1777 (2016).
13. Wooller, M. J. *et al.* Reconstruction of past methane availability in an Arctic Alaska wetland indicates climate influenced methane release during the past ~12,000 years. *J Paleolimnol* **48**, 27–42 (2012).
14. McFarlin, J. M., Axford, Y., Masterson, A. L. & Osburn, M. R. Calibration of modern sedimentary $\delta^2\text{H}$ plant wax-water relationships in Greenland lakes. *Quat Sci Rev* **225**, 105978 (2019).

15. Liebner, S. *et al.* Methane oxidation associated with submerged brown mosses reduces methane emissions from Siberian polygonal tundra. *Journal of Ecology* **99**, 914–922 (2011).
16. Raghoebarsing, A. A. *et al.* Methanotrophic symbionts provide carbon for photosynthesis in peat bogs. *Nature* **436**, 1153–1156 (2005).
17. Bush, R. T. & McInerney, F. A. Leaf wax n-alkane distributions in and across modern plants: Implications for paleoecology and chemotaxonomy. *Geochim Cosmochim Acta* **117**, 161–179 (2013).
18. Sachse, D. *et al.* Molecular Paleohydrology: Interpreting the Hydrogen-Isotopic Composition of Lipid Biomarkers from Photosynthesizing Organisms. *Annu Rev Earth Planet Sci* **40**, 221–249 (2012).
19. McFarlin, J. M. *et al.* Pronounced summer warming in northwest Greenland during the Holocene and Last Interglacial. *Proceedings of the National Academy of Sciences* **115**, 6357–6362 (2018).
20. Kusch, S. *et al.* Holocene environmental history in high-Arctic North Greenland revealed by a combined biomarker and macrofossil approach. *Boreas* **48**, 273–286 (2019).
21. Thomas, E. K., Briner, J. P., Ryan-Henry, J. J. & Huang, Y. A major increase in winter snowfall during the middle Holocene on western Greenland caused by reduced sea ice in Baffin Bay and the Labrador Sea. *Geophys Res Lett* **43**, 5302–5308 (2016).
22. Thomas, E. K., Hollister, K. v., Cluett, A. A. & Corcoran, M. C. Reconstructing Arctic Precipitation Seasonality Using Aquatic Leaf Wax $\delta^2\text{H}$ in Lakes With Contrasting Residence Times. *Paleoceanogr Paleoclimatol* **35**, e2020PA003886 (2020).
23. Axford, Y. *et al.* Holocene temperature history at the western Greenland Ice Sheet margin reconstructed from lake sediments. *Quat Sci Rev* **59**, 87–100 (2013).
24. Sand-Jensen, K., Riis, T., Markager, S. & Vincent, W. F. Slow growth and decomposition of mosses in Arctic lakes. *Canadian Journal of Fisheries and Aquatic Sciences* **56**, 388–393 (1999).
25. Lecavalier, B. S. *et al.* High Arctic Holocene temperature record from the Agassiz ice cap and Greenland ice sheet evolution. *Proc Natl Acad Sci U S A* **114**, 5952–5957 (2017).
26. Vinther, B. M. *et al.* Holocene thinning of the Greenland ice sheet. *Nature* **461**, 385–388 (2009).
27. Kahmen, A. *et al.* Leaf water deuterium enrichment shapes leaf wax n-alkane δD values of angiosperm plants II: Observational evidence and global implications. *Geochim Cosmochim Acta* **111**, 50–63 (2013).
28. Axford, Y., Osterberg, E. C. & de Vernal, A. Past warmth and its impacts in Greenland during the Holocene Thermal Maximum. *Annu Rev Earth Planet Sci* **49**, 279–307 (2021).
29. Bowen, G. J. The Online Isotopes in Precipitation Calculator, version 3.1. http://wateriso.utah.edu/waterisotopes/pages/data_access/oipc.html (2020).
30. IAEA/WMO. Global Network of Isotopes in Precipitation. The GNIP Database. (2020).
31. Bowen, G. J., Wassenaar, L. I. & Hobson, K. A. Global application of stable hydrogen and oxygen isotopes to wildlife forensics. *Oecologia* **143**, 337–348 (2005).
32. Corcoran, M. C., Thomas, E. K. & Morrill, C. Using a Paired Chironomid $\delta^{18}\text{O}$ and Aquatic Leaf Wax $\delta^2\text{H}$ Approach to Reconstruct Seasonality on Western Greenland During the Holocene. *Paleoceanogr Paleoclimatol* **36**, 1–18 (2021).
33. Hanna, E., Mernild, S. H., Cappelen, J. & Steffen, K. Recent warming in Greenland in a long-term instrumental (1881–2012) climatic context: I. Evaluation of surface air temperature records. *Environmental Research Letters* **7**, 045404 (2012).
34. Mernild, S. H. *et al.* Greenland precipitation trends in a long-term instrumental climate context (1890–2012): evaluation of coastal and ice core records. *International Journal of Climatology* **35**, 303–320 (2015).
35. Oliver, D. R. Life History of the Chironomidae. *Annu Rev Entomol* **16**, 211–230 (1971).
36. van Hardenbroek, M. *et al.* The stable isotope composition of organic and inorganic fossils in lake sediment records : Current understanding , challenges , and future directions. *Quat Sci Rev* **196**, 154–176 (2018).

37. Lasher, G. E. *et al.* Holocene temperatures and isotopes of precipitation in Northwest Greenland recorded in lacustrine organic materials. *Quat Sci Rev* **170**, 45–55 (2017).
38. Blaga, C. I., Reichart, G.-J., Heiri, O. & Sinninghe Damsté, J. S. Tetraether membrane lipid distributions in water-column particulate matter and sediments: a study of 47 European lakes along a north–south transect. *J Paleolimnol* **41**, 523–540 (2009).
39. Lattaud, J., de Jonge, C., Elling, F. J., Pearson, A. & Eglinton, T. I. *Microbial lipid signatures in Arctic deltaic sediments - insight into methane cycling and climate variability*. *Earth ArXiv* (2020) doi:https://doi.org/10.31223/X5B01W.
40. Tierney, J. E. GDGT Thermometry: Lipid Tools for Reconstructing Paleotemperatures. in *Reconstructing Earth's Deep-Time Climate--The State of the Art in 2012* 115–131 (2012).
41. Kip, N. *et al.* Global prevalence of methane oxidation by symbiotic bacteria in peat-moss ecosystems. *Nat Geosci* **3**, 617–621 (2010).
42. Basiliko, N., Knowles, R. & Moore, T. R. Roles of moss species and habitat in methane consumption potential in a northern peatland. *Wetlands* **24**, 178–185 (2004).
43. Zibulski, R. *et al.* C / N ratio, stable isotope ($\delta^{13}\text{C}$, $\delta^{15}\text{N}$), and n-alkane patterns of brown mosses along hydrological gradients of low-centred polygons of the Siberian Arctic. *Biogeosciences* **14**, 1617–1630 (2017).
44. Knoblauch, C., Spott, O., Evgrafova, S., Kutzbach, L. & Pfeiffer, E. Regulation of methane production, oxidation, and emission by vascular plants and bryophytes in ponds of the northeast Siberian polygonal tundra. *J Geophys Res Biogeosci* **120**, 2525–2541 (2015).
45. Larmola, T. *et al.* Methanotrophy induces nitrogen fixation during peatland development. *Proceedings of the National Academy of Sciences* **111**, 734–739 (2014).
46. Larmola, T. *et al.* The role of Sphagnum mosses in the methane cycling of a boreal mire. *Ecology* **91**, 2356–2365 (2010).
47. Guo, C. Q. *et al.* Warnstorfia exannulata, an aquatic moss in the Arctic: Seasonal growth responses. *Clim Change* **119**, 407–419 (2013).
48. Riis, T. & Sand-Jensen, K. Growth Reconstruction and Photosynthesis of Aquatic Mosses: Influence of Light, Temperature and Carbon Dioxide at Depth. *Journal of Ecology* **85**, 359–372 (1997).
49. Wagner, B. & Bennike, O. Holocene environmental change in the Skallingen area, eastern North Greenland, based on a lacustrine record. *Boreas* **44**, 45–59 (2015).
50. Chanton, J. P., Fields, D. & Hines, M. E. Controls on the hydrogen isotopic composition of biogenic methane from high-latitude terrestrial wetlands. *J Geophys Res Biogeosci* **111**, (2006).
51. Brosius, L. S. *et al.* Using the deuterium isotope composition of permafrost meltwater to constrain thermokarst lake contributions to atmospheric CH₄ during the last deglaciation. *J Geophys Res Biogeosci* **117**, (2012).
52. van Winden, J. F. *et al.* Lipids of symbiotic methane-oxidizing bacteria in peat moss studied using stable carbon isotopic labelling. *Org Geochem* **41**, 1040–1044 (2010).
53. van Winden, J. F. *et al.* Influence of temperature on the $\delta^{13}\text{C}$ values and distribution of methanotroph-related hopanoids in Sphagnum dominated peat bogs. *Geobiology* **18**, 497–507 (2020).
54. Cadieux, S. B., White, J. R. & Pratt, L. M. Exceptional summer warming leads to contrasting outcomes for methane cycling in small Arctic lakes of Greenland. *Biogeosciences* **14**, 559–574 (2017).
55. Juutinen, S. *et al.* Methane dynamics in different boreal lake types. *Biogeosciences* **6**, 209–223 (2009).
56. Cadieux, S. B. *et al.* Large fractionations of C and H isotopes related to methane oxidation in Arctic lakes. *Geochim Cosmochim Acta* **187**, 141–155 (2016).
57. Saros, J. E., Northington, R. M., Osburn, C. L., Burpee, B. T. & John Anderson, N. Thermal stratification in small arctic lakes of southwest Greenland affected by water transparency and epilimnetic temperatures. *Limnol Oceanogr* **61**, 1530–1542 (2016).

58. Northington, R. M. & Saros, J. E. Factors Controlling Methane in Arctic Lakes of Southwest Greenland. *PLoS One* **11**, e0159642 (2016).
59. Fritz, S. C. & Anderson, N. J. The relative influences of climate and catchment processes on Holocene lake development in glaciated regions. *J Paleolimnol* **49**, 349–362 (2013).
60. Liu, X., Colman, S. M., Brown, E. T., Minor, E. C. & Li, H. Estimation of carbonate, total organic carbon, and biogenic silica content by FTIR and XRF techniques in lacustrine sediments. *J Paleolimnol* **50**, 387–398 (2013).
61. Reig, F. FTIR quantitative analysis of calcium carbonate (calcite) and silica (quartz) mixtures using the constant ratio method. Application to geological samples. *Talanta* **58**, 811–821 (2002).
62. Xia, M., Yao, Z., Ge, L., Chen, T. & Li, H. A potential bio-filler: The substitution effect of furfural modified clam shell for carbonate calcium in polypropylene. *J Compos Mater* **49**, 807–816 (2015).
63. Rach, O., Kahmen, A., Brauer, A. & Sachse, D. A dual-biomarker approach for quantification of changes in relative humidity from sedimentary lipid D/H ratios. *Climate of the Past* **13**, 741–757 (2017).
64. Balascio, N. L., D'Andrea, W. J., Bradley, R. S. & Perren, B. B. Biogeochemical evidence for hydrologic changes during the Holocene in a lake sediment record from southeast Greenland. *Holocene* **23**, 1428–1439 (2013).
65. Curtin, L. *et al.* Holocene and Last Interglacial climate of the Faroe Islands from sedimentary plant wax hydrogen and carbon isotopes. *Quat Sci Rev* **223**, 105930 (2019).
66. Balascio, N. L., D'Andrea, W. J., Anderson, R. S. & Wickler, S. Influence of vegetation type on n-alkane composition and hydrogen isotope values from a high latitude ombrotrophic bog. *Org Geochem* **121**, 48–57 (2018).
67. Dion-Kirschner, H., McFarlin, J. M., Masterson, A. L., Axford, Y. & Osburn, M. R. Modern constraints on the sources and climate signals recorded by sedimentary plant waxes in west Greenland. *Geochim Cosmochim Acta* **286**, 336–354 (2020).
68. Aichner, B., Herzsuh, U., Wilkes, H., Vieth, A. & Böhner, J. δD values of n-alkanes in Tibetan lake sediments and aquatic macrophytes – A surface sediment study and application to a 16ka record from Lake Koucha. *Org Geochem* **41**, 779–790 (2010).
69. Yakir, D. & DeNiro, M. J. Oxygen and Hydrogen Isotope Fractionation during Cellulose Metabolism in *Lemna gibba* L. *Plant Physiol* **93**, 325–332 (1990).
70. Aichner, B., Hilt, S., Périllon, C., Gillefalk, M. & Sachse, D. Biosynthetic hydrogen isotopic fractionation factors during lipid synthesis in submerged aquatic macrophytes: Effect of groundwater discharge and salinity. *Org Geochem* **113**, 10–16 (2017).
71. Glime, J. Nutrient Relations: CO₂. in *Bryophyte Ecology* (2017).
72. Axford, Y. *et al.* Holocene temperature history of northwest Greenland – With new ice cap constraints and chironomid assemblages from Deltasø. *Quat Sci Rev* **215**, 160–172 (2019).
73. Axford, Y. *et al.* Timing and magnitude of early to middle Holocene warming in East Greenland inferred from chironomids. *Boreas* **46**, 678–687 (2017).

Acknowledgments

We thank the people and Government of Greenland (sample export permit 028/2014), the Thule Air Base, Air Greenland, the US Air Force, the Air National Guard, and Polar Field Services for logistical support. M. Kelly, E. Osterberg, A. Taylor, G. Bromley, M. Jackson, L. Farnsworth assisted with field work. H. Dion-Kirshner, J. Todes, S. Lee provided laboratory assistance. Sebastian Kopf provided helpful feedback on this manuscript. Published data was obtained from the NOAA paleoclimate database and we thank our

colleagues for sharing data there. Map was created using The Generic Mapping Tools (GMT). Funding sources include NSF Division of Polar Programs (Awards 1108306, 1107411, 1454734), NSF-GRF awarded to J.M.M.; Northwestern University (NU) ISEN Award to Y.A., NU ISEN Award to M.R.O.; GSA Graduate Student Research Award to J.M.M.

Author contributions: J.M.M., Y.A., M.R.O. designed research; J.M.M., M.R.O., S.K., G.E.L., A.M., performed research; J.M.M., M.R.O., Y.A., S.K. analyzed data; J.M.M., Y.A., M.R.O., S.K. wrote the paper

Competing Interests: Authors declare no competing interests.

Materials & Correspondence: Inquiries regarding this manuscript and material requests should be addressed to Dr. Jamie McFarlin at jamie.mcfarlin@uwyo.edu

Figures

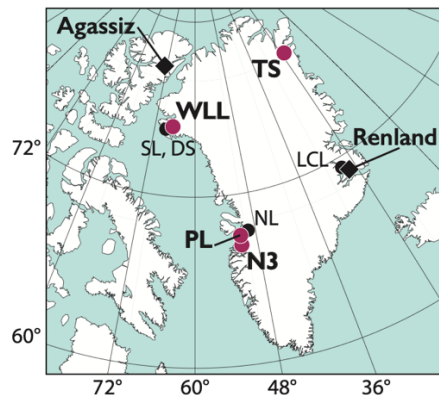


Figure 1. Map of Greenland with sites discussed in text. Red circles are lakes with sedimentary plant wax isotope data included here. Black circles are lakes with published temperature reconstructions referenced in the text. Black diamonds represent locations of ice core records discussed in this text. Lake name abbreviations: WLL= Wax Lips Lake¹⁹, TS = Trifna Sø²⁰, N3 = Lake N3²¹, PL = Pluto Lake²², SL = Secret Lake³⁷, DS = Delta Sø⁷², NL = North Lake²³, LCL = Last Chance Lake⁷³.

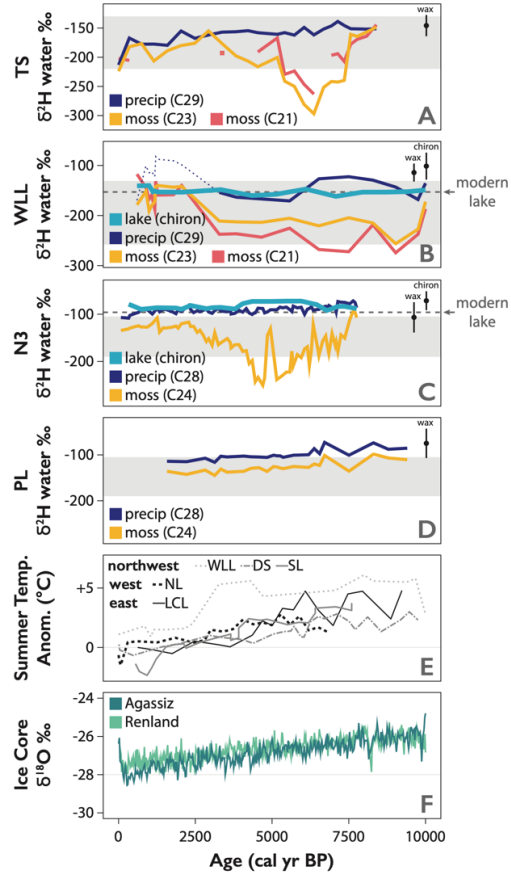


Figure 2. Holocene reconstructed water isotopes and climate at A) TS, with estimated $\delta^2\text{H}_{\text{precip}}$ values (dark blue) from long-chain alkanes and estimated $\delta^2\text{H}_{\text{moss}}$ values (orange, red) from mid-chain alkanes, B) WLL, with estimated $\delta^2\text{H}_{\text{precip}}$ values (dark blue) from long-chain alkanes, estimated $\delta^2\text{H}_{\text{lake}}$ values from chironomid chitin (bright blue), and estimated $\delta^2\text{H}_{\text{moss}}$ values (orange, red) from mid-chain alkanes, C) N3, with estimated $\delta^2\text{H}_{\text{precip}}$ values (dark blue) from long-chain alkanoic acids, estimated $\delta^2\text{H}_{\text{lake}}$ values from chironomid chitin (bright blue), and estimated $\delta^2\text{H}_{\text{moss}}$ values (orange) from mid-chain alkanoic acids, D) PL, with estimated $\delta^2\text{H}_{\text{precip}}$ values (dark blue) from long-chain alkanoic acids and estimated $\delta^2\text{H}_{\text{moss}}$ values (orange) from mid-chain alkanoic acids, E) summer air temperature anomalies relative to 20th century (pre-1950) from lakes on northwest (WLL, SL, DS), west (NL), and east Greenland (LCL), and G) $\delta^{18}\text{O}_{\text{ice}}$ values from the nearby Agassiz (dark green) and Renland (light green) ice caps. Gray bands in A-D encompass the range of modern precipitation isotopes at each site (upper bound = most enriched summer month, lower bound = most depleted winter month), estimated using the OIPC²⁹. Dotted black line in B and C shows the measured modern $\delta^2\text{H}_{\text{lakewater}}$ value. Error bars in upper right of A-D represent the average point propagated error for estimates on wax and chironomid water isotope reconstructions respectively, including 1 σ error from the calibration data and analytical error on the measurements.

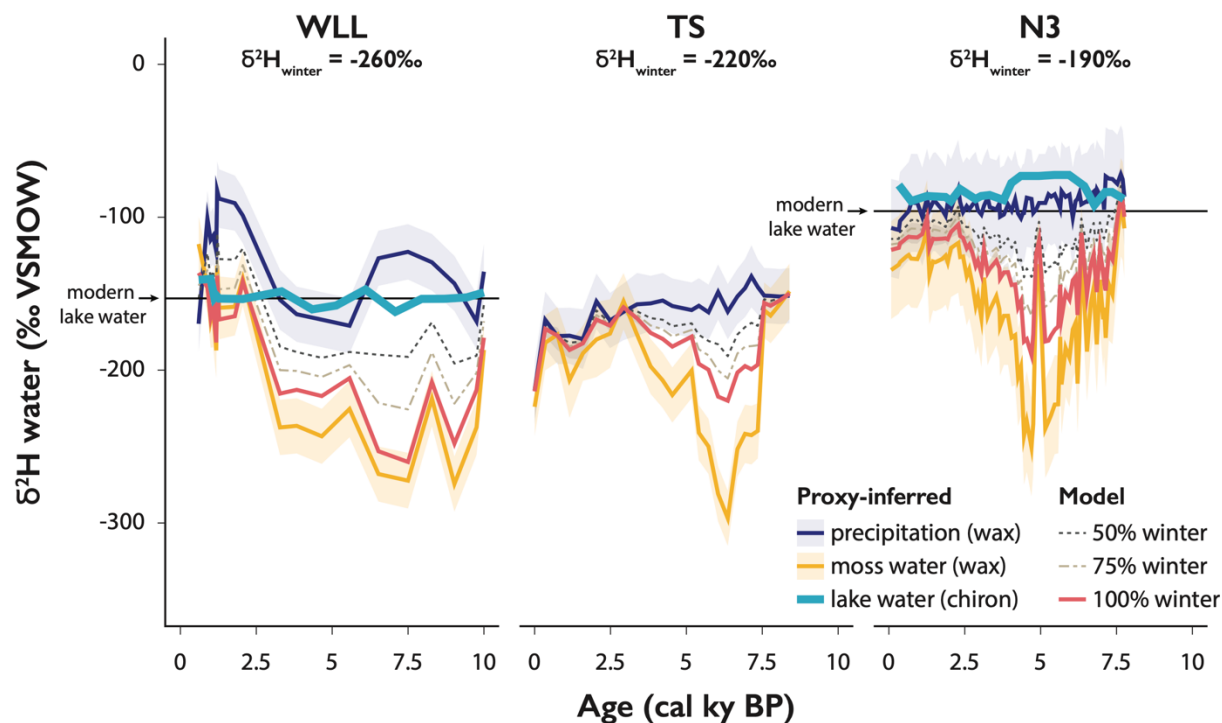


Figure 3. Hydrogen isotope mass balance models for WLL, TS, and N3 demonstrating proxy-inferred $\delta^2\text{H}_{\text{precip}}$ values (WLL, TS, N3; dark blue), proxy-inferred $\delta^2\text{H}_{\text{lakewater}}$ values (WLL, N3; bright blue), proxy-inferred $\delta^2\text{H}_{\text{moss water}}$ values (WLL, TS, N3; orange), and modeled $\delta^2\text{H}$ values of lake water using 100% winter endmember precipitation (red, solid), 75% winter endmember precipitation (light brown, dashed), and 50% winter endmember precipitation (charcoal, dotted) input into the model as maximum contribution to lake water when short-chain waxes are most depleted relative to long-chain wax (see Methods).

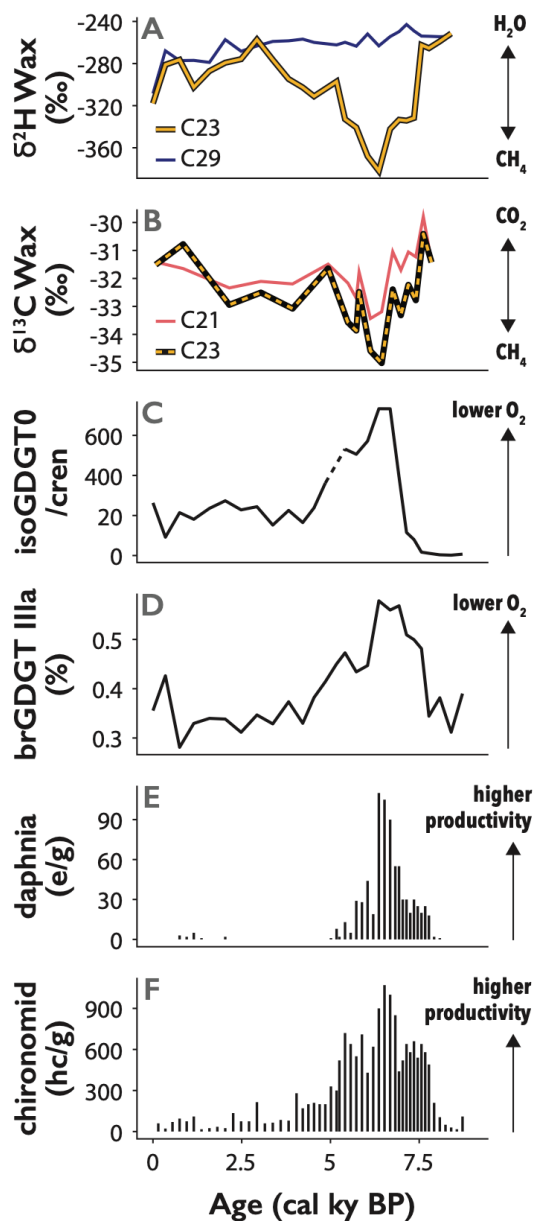


Figure 4. Holocene proxy data from TS showing A) $\delta^2\text{H}_{\text{wax}}$ values of sedimentary long-chain (C₂₉; dark-blue) and mid-chain (C₂₃; orange) alkanes, B) $\delta^{13}\text{C}_{\text{wax}}$ values of sedimentary mid-chain (C₂₁, red; C₂₃, dashed orange and black) alkanes, C) ratio of isoGDGT-0:crenarchaeol (higher values indicate lower O₂), D) fractional abundance of brGDGT IIIa (%) (higher values indicate lower O₂), concentration of E) aquatic invertebrate remains from *Daphnia* in ephippia per gram dry sediment (e/g) (higher values indicate higher productivity) and F) chironomid larvae in head capsules per gram dry sediment (hc/g)²⁰ (higher values indicate higher productivity).

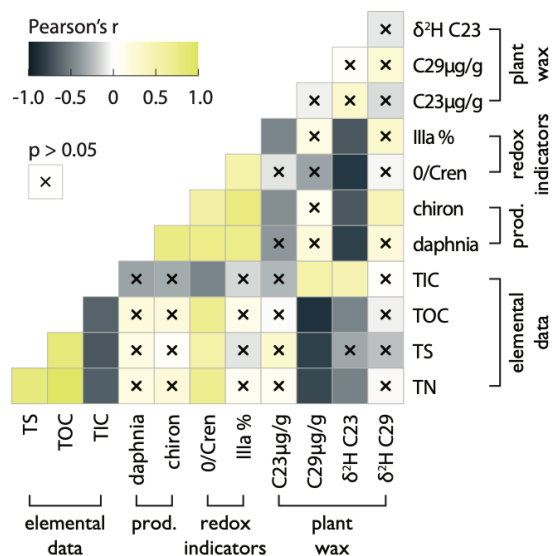


Figure S1. Correlation matrix showing Pearson's r between variables at TS with proxy data grouped by category: elemental data, including total nitrogen (TN), total sulfur (TS), total organic carbon (TOC), and total inorganic carbon (TIC); indicators of general productivity rates ("prod."), including abundances of ephippia of *Daphnia* carapaces and chironomid head capsules per gram sediment; redox indicators sensitive to hypolimnetic oxygen, including the ratio of isoGDGT-0/crenarchaeol (0/cren), fractional abundances of brGDGT IIIa as a percent relative to all brGDGT isomers (IIIa %); and plant wax biomarkers, including abundance of C_{23} and C_{29} n -alkanes in $\mu\text{g/g}$ TOC, and $\delta^2\text{H}$ values of C_{23} and C_{29} n -alkanes; where dark gray represents $r = -1$, white represents $r = 0$, bright yellow represents $r = 1$, and an x over the box indicates the relationship is not significant ($p > 0.05$).

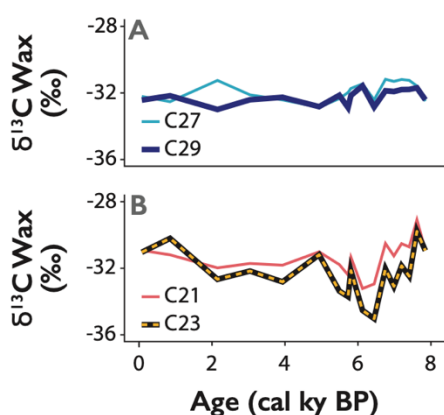


Figure S2. Holocene carbon isotopic composition of A) long-chain (C_{27} and C_{29}) and B) mid-chain (C_{21} and C_{23}) alkanes from TS in permil relative to VPDB-LVSEC.

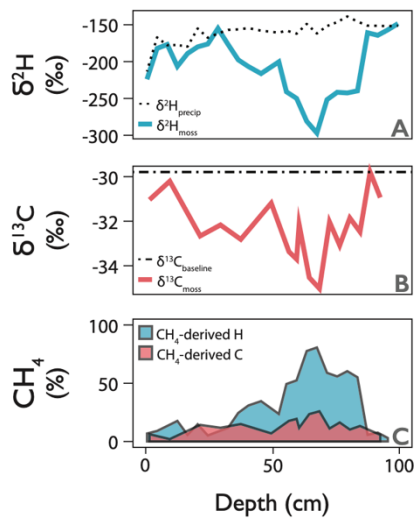


Figure S3. Hydrogen and carbon isotope mass balance models for TS demonstrating, A) proxy-inferred $\delta^2\text{H}_{\text{precip}}$ values (C_{29} , dotted black) and proxy-inferred $\delta^2\text{H}_{\text{moss}}$ water values (C_{23} ; bright blue), B) $\delta^{13}\text{C}$ values of mid-chain wax (pink) and selected $\delta^{13}\text{C}$ baseline pre- and post-depletion (dashed black), and C) modeled % input of CH_4 -derived H (blue) and CH_4 -derived C (pink) to moss biomass (see Methods).

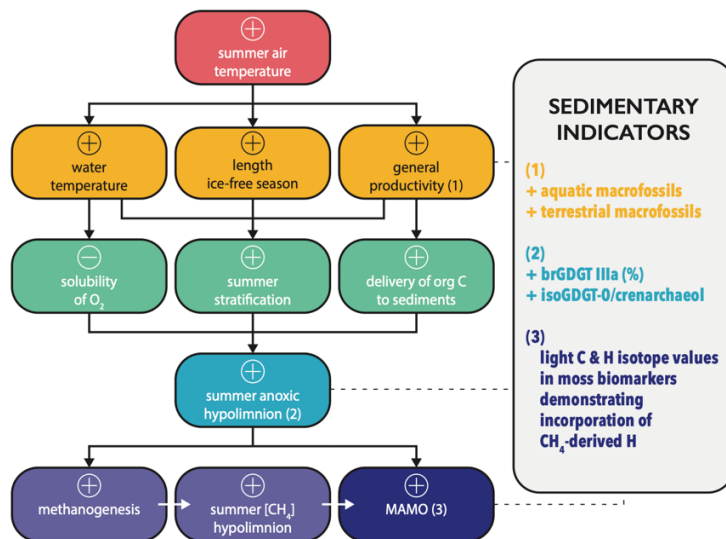


Figure S4. Flow chart of the proposed system changes hypothesized for TS, WLL, and N3 driven by warming air temperatures in the early-middle Holocene. Dashed lines identify areas where proxy data from TS provide a sedimentary indicator of that change, with those indicators listed by number in gray panel on the right. + symbols denote an increase or strengthening of variable, - symbol denotes a decrease or weakening of variable, $[\text{CH}_4]$ = concentration of methane, MAMO = moss-associated methane oxidation.